J|A|C|S
ARTICLES
Published on Web 12/09/2006

Comparing the Electronic Properties of the Low-Spin Cyano−Ferric [Fe(N$_4$)(Cys)] Active Sites of Superoxide Reductase and P450cam Using ENDOR Spectroscopy and DFT Calculations

Tran-Chin Yang,[II] Rebecca L. McNaughton,[II] Michael D. Clay,[§] Francis E. Jenney, Jr.,[‡] Rangan Krishnan,[§] Donald M. Kurtz, Jr.,[†] Michael W. W. Adams,[‡] Michael K. Johnson,[§] and Brian M. Hoffman*,[II]

Contribution from the Departments of Chemistry and Biochemistry and Molecular Biology, and the Center for Metalloenzyme Studies, University of Georgia, Athens, Georgia 30602, Department of Chemistry, University of Texas at San Antonio, San Antonio, Texas 78249, and Department of Chemistry, Northwestern University, Evanston, Illinois 60208

Received June 30, 2006; E-mail: bmh@northwestern.edu

Abstract: Superoxide reductase (SOR) and P450 enzymes contain similar [Fe(N)$_4$(S$_{Cys}$)] active sites and, although they catalyze very different reactions, are proposed to involve analogous low-spin (hydro)peroxo-Fe(III) intermediates in their respective mechanisms that can be modeled by cyanide binding. The equatorial FeN$_4$ ligation by four histidine ligands in CN-SOR and the heme in CN-P450cam is directly compared by ^{14}N ENDOR, while the axial Fe−CN and Fe−S bonding is probed by ^{13}C ENDOR of the cyanide ligand and ^{1}H$_\beta$ ENDOR measurements to determine the spin density delocalization onto the cysteine sulfur. There are small, but notable, differences in the bonding between Fe(III) and its ligands in the two enzymes. The ENDOR measurements are complemented by DFT computations that support the semiempirical equation used to compute spin densities on metal-coordinated cysteinyl and shed light on bonding changes as the Fe−C−N linkage bends. They further indicate that H bonds to the cysteinyl thiolate sulfur ligand reduce the spin density on the sulfur in both active sites to a degree that exceeds the difference induced by the alternative sets of "in-plane" nitrogen ligands.

Introduction

Superoxide reductases (SORs) are non-heme iron enzymes that scavenge superoxide in anaerobic bacteria and archaea by the one-electron reduction of superoxide to hydrogen peroxide, rather than the classical disproportionation of superoxide to hydrogen peroxide and dioxygen catalyzed by the well-known superoxide dismutases.[1−6] The X-ray crystal structures of SORs from the hyperthermophilic archaeon *Pyrococcus furiosus*[7] and the microaerophilic sulfate reducing bacterium *Desulfovibrio desulfuricans*[8] disclose a common [Fe(N$_{His}$)$_4$(S$_{Cys}$)] active site, with nitrogen ligands from four histidyl imidazoles forming a pseudo square plane and a cysteinyl thiolate providing an endogenous "axial" ligand. This N$_4$S endogenous ligand set evokes the coordination sphere of P450 monooxygenases, in which the heme-iron active center is coordinated by four pyrrole nitrogens from porphyrin and one axial cysteinyl sulfur. The basic structural similarity of these distinct Fe[N$_4$S] centers is illustrated by the overlap of their structures in Figure 1.

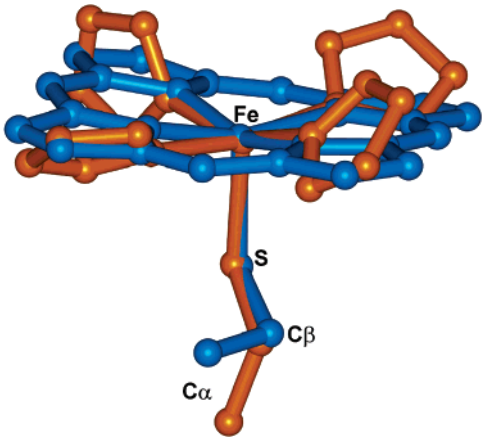

Figure 1. Overlay of the Fe(N$_4$S$_{Cys}$) active sites of SOR and P450cam.

[§] Department of Chemistry, University of Georgia.
[‡] Department of Biochemistry & Molecular Biology, University of Georgia.
[†] Department of Chemistry, University of Texas at San Antonio.
[II] Department of Chemistry, Northwestern University.

(1) Jenney, F. E., Jr.; Verhagen, M. F. J. M.; Cui, X.; Adams, M. W. W. *Science* **1999**, *286*, 306−309.
(2) Adams, M. W. W.; Jenney, F. E., Jr.; Clay, M. D.; Johnson, M. K. *J. Biol. Inorg. Chem.* **2002**, *7*, 647−652.
(3) Abreu, I. A.; Xavier, A. V.; LeGall, J.; Cabelli, D. E.; Teixeira, M. *J. Biol. Inorg. Chem.* **2002**, *7*, 668−674.
(4) Imlay, J. A. *J. Biol. Inorg. Chem.* **2002**, *7*, 659−663.
(5) Niviere, V.; Fontecave, M. *J. Biol. Inorg. Chem.* **2004**, *9*, 119−123.
(6) Kurtz, D. M., Jr. *Acc. Chem. Res.* **2004**, *37*, 902−908.
(7) Yeh, A. P.; Hu, Y.; Jenney, F. E., Jr.; Adams, M. W.; Rees, D. C. *Biochemistry* **2000**, *39*, 2499−2508.
(8) Coelho, A. V.; Matias, P.; Fulop, V.; Thompson, A.; Gonzalez, A.; Carrondo, M. A. *J. Biol. Inorg. Chem.* **1997**, *2*, 680−689.

10.1021/ja064656p CCC: $33.50

Scheme 1

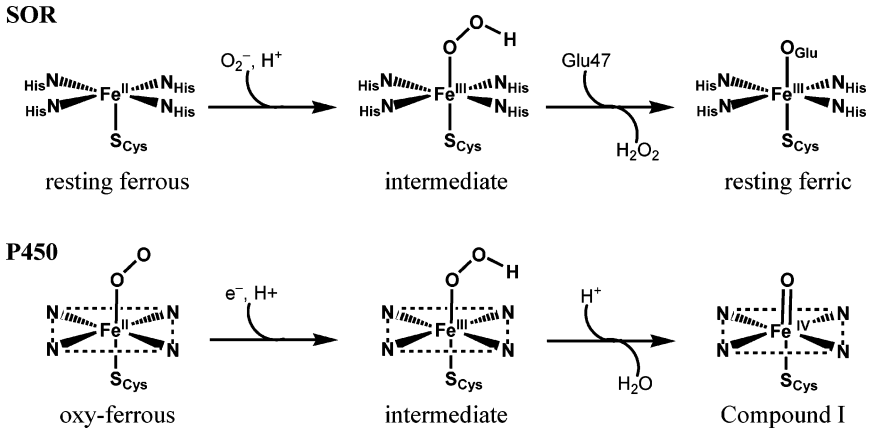

SOR and P450 not only have active sites with the same first-shell coordination spheres, they are thought to share a common ferric-(hydro)peroxy catalytic intermediate even though they catalyze very different reactions. P450 catalyzes O_2 activation and heterolytic O−O bond cleavage to yield a high-valent Fe^{IV}═O oxidizing species via a proposed low-spin Fe(III)-OOH intermediate,[9,10] whereas SOR catalyzes reduction of O_2^- to H_2O_2 without O−O bond cleavage (Scheme 1).[1,6,11] Cyanide forms low-spin complexes with both the ferric SOR site[12−14] and the ferric site of P450,[15] with the cyanide carbon-coordinated *trans* to the cysteinyl sulfur, mimicking the putative ferric-(hydro)peroxo intermediates in the reactions of both enzymes. A comparison of the properties of the cyanoferric-SOR and cyanoferric-P450cam should provide insights into the differences between "in-plane" N_4[heme] and N_4[His] coordination to iron, with the common thiolate (cysteinate) and cyanide axial ligands serving as ENDOR and vibrational probes of the influence of the different in-plane N_4 ligands on iron-axial ligand bonding interactions.

The Fe−S bonding in the ferric-SOR active site has unusual features that appear to be more similar to those of blue copper centers than to those of hemes.[7,8,13,16−20] In both cases, the metal (M) has a highly covalent σ bond to cysteinyl sulfur and as well as π-type overlap between the ground-state odd-electron d orbital and the p_π orbital of sulfur, a near planar M−S−C_β−C_α−N unit for the coordinated cysteine, and an intense absorption band in the visible region near 600 nm, corresponding to a S(p_π) → M(d_π) charge-transfer transition. In blue copper centers, it was found that extensive delocalization of the odd electron onto the cysteinyl sulfur generates strong isotropic hyperfine coupling, a_{iso} > 20 MHz, to at least one of the two β protons,[21−23] but such a direct test of Fe−S spin delocalization in ferric-SOR has not been carried out. Likewise, although the role of the axial thiolate in P450 chemistry has been extensively discussed, the Fe−S spin delocalization in ferric-P450cam has not been examined by experiment.

Recently, we reported the results of resonance Raman, FTIR, and[14,15]N- and ^{13}C ENDOR studies of the cyano-ferric and -ferrous complexes of wild-type (WT) and variant forms of *P. furiosus* 1Fe-SOR and *Desulfovibrio vulgaris* 2Fe-SOR.[24] The cyanoferric-SORs were shown to exhibit three distinct active-site conformations that differ in the Fe−C−N angle and spin delocalization onto CN. Resonance Raman studies of WT and variant forms of cyano-ferri-P450cam have been reported,[25,26] but spin delocalization information is not available.

To explore the similarities and differences in the electronic structures of the SOR and P450cam active sites we report here the results of ENDOR studies designed to compare the cyano-ferric states of P450cam with those of WT *P. furiosus* 1Fe-SOR and the WT and C13S mutant forms of *D. vulgaris* 2Fe-SOR (the mutation results in removal of a spectroscopically interfering [Fe(S_{Cys})$_4$] site with no detectable effect on activity[27]). Specifically, the equatorial FeN_4 ligation in the heme of P450s and the equatorial iron ligation by four histidine ligands in SORs are compared directly by ^{14}N ENDOR, while the axial Fe−S and Fe−CN bonding is probed by ^{1}H ENDOR measurements of spin density delocalization onto the cysteine sulfur and ^{13}C ENDOR measurements to compare the mode of cyanide bonding. DFT computations have been carried out in parallel with the spectroscopic studies to examine and expand on the experimental findings. Taken together, the ENDOR and computational results show that H bonds to the cysteinyl thiolate

(9) Davydov, R.; Makris, T. M.; Kofman, V.; Werst, D. W.; Sligar, S. G.; Hoffman, B. M. *J. Am. Chem. Soc.* **2001**, *123*, 1403−1415.
(10) Schlichting, I.; Berendzen, J.; Chu, K.; Stock, A. M.; Maves, S. A.; Benson, D. E.; Sweet, B. M.; Ringe, D.; Petsko, G. A.; Sligar, S. G. *Science* **2000**, *287*, 1615−1622.
(11) Lombard, M.; Fontecave, M.; Touati, D.; Niviere, V. *J. Biol. Chem.* **2000**, *275*, 115−121.
(12) Romao, C. V.; Liu, M. Y.; Le, Gall, J.; Gomes, C. M.; Braga, V.; Pacheco, I.; Xavier, A. V.; Teixeira, M. *Eur. J. Biochem.* **1999**, *261*, 438−443.
(13) Clay, M. D.; Jenney, F. E., Jr.; Hagedoorn, P. L.; George, G. N.; Adams, M. W. W.; Johnson, M. K. *J. Am. Chem. Soc.* **2002**, *124*, 788−805.
(14) Silva, G.; Oliveira, S.; Gomes, C. M.; Pacheco, I.; Liu, M. Y.; Xavier, A. V.; Teixeira, M.; LeGall, J.; Rodrigues-Pousada, C. *Eur. J. Biochem.* **1999**, *259*, 235−243.
(15) Fedorov, R.; Ghosh, D. K.; Schlichting, I. *Arch. Biochem. Biophys.* **2003**, *409*, 25−31.
(16) Guss, J. M.; Freeman, H. C. *J. Mol. Biol.* **1983**, *169*, 521−563.
(17) Norris, G. E.; Anderson, B. F.; Baker, E. N. *J. Am. Chem. Soc.* **1986**, *108*, 2784−2785.
(18) Solomon, E. I.; Lowery, M. D. *Science* **1993**, *259*, 1575−1581.
(19) Gewirth, A. A.; Solomon, E. I. *J. Am. Chem. Soc.* **1988**, *110*, 3811−3819.
(20) Clay, M. D.; Cosper, C. A.; Jenney, F. E., Jr.; Adams, M. W. W.; Johnson, M. K. *Proc. Natl. Acad. Sci. U.S.A.* **2003**, *100*, 3796−3801.
(21) Werst, M. M.; Davoust, C. E.; Hoffman, B. M. *J. Am. Chem. Soc.* **1991**, *113*, 1533−1538.
(22) Roberts, J. E.; Cline, J. F.; Lum, V.; Freeman, H.; Gray, H. B.; Peisach, J.; Reinhammar, B.; Hoffman, B. M. *J. Am. Chem. Soc.* **1984**, *106*, 5324−5330.
(23) Coremans, J. W. A.; Poluektov, O. G.; Groenen, E. J. J.; Canters, G. W.; Nar, H.; Messerschmidt, A. *J. Am. Chem. Soc.* **1997**, *119*, 4726−4731.
(24) Clay, M. D.; Yang, T.-C.; Jenney, F. E., Jr.; Kung, I. Y.; Cosper, C. A.; Krishnan, R.; Kurtz, D. M., Jr.; Adams, M. W. W.; Hoffman, B. M.; Johnson, M. K. *Biochemistry* **2006**, *45*, 427−438.
(25) Simianu, M. C.; Kincaid, J. R. *J. Am. Chem. Soc.* **1995**, *117*, 4628−4636.
(26) Deng, T.-J.; Macdonald, I. D. G.; Simianu, M. C.; Sykora, M.; Kincaid, J. R.; Sligar, S. G. *J. Am. Chem. Soc.* **2001**, *123*, 269−278.
(27) Emerson, J. P.; Cabelli, D. E.; Kurtz, D. M., Jr. *Proc. Natl. Acad. Sci. U.S.A.* **2003**, *100*, 3802−3807.

sulfur play a significant role in tuning the bonding between iron and the axial cysteinyl ligand.

Materials and Methods

Materials. Samples of cyano-ferri-SOR[24] and cyano-ferri-P450cam[28] were prepared as described elsewhere.

ENDOR Spectroscopy. Q-band continuous wave (CW) ^{1}H and ^{14}N ENDOR spectra were acquired at 2 K on a spectrometer described previously.[21] Q-band ^{1}H pulsed ENDOR spectra were collected on a spectrometer described previously.[29] The radio frequency (RF) was bandwidth broadened to 100 kHz to increase the signal-to-noise ratio. As discussed elsewhere, the sign of the ^{1}H hyperfine couplings from the cysteinyl β protons were determined from the pulsed ENDOR peak intensities and phases as collected with a modified Davies/Hahn (D/H) spin−echo ENDOR pulse train,[30] (Chart 1)

Chart 1

$$\{\pi/2, [\tau_R, t_{RF}, \pi/2, \tau, \pi]_n, \tau, \text{echo}\}$$

where $\pi/2$ and π represent microwave pulses that "turn" the resonant electron spins by those angles, $\tau_R \gg \tau$ are delay times, the RF field is applied during t_{RF} (= 100 μs typically), and n represents a large number of repetitions.

For a proton ($I = {}^1/_2$), the ENDOR pattern to a first-order approximation is given by

$$\nu_\pm = |\nu_n \pm A/2| \quad (1)$$

where ν_n is the nuclear Larmor frequency, and A is the orientation-dependent hyperfine coupling constant. When $\nu_n > |A/2|$ as is the case here for ^{1}H ENDOR, the two branches, $\nu_\pm$, are separated by $|A/2|$ and centered at ν_n. When $\nu_n < |A/2|$, as for strongly coupled ^{14}N, $\nu_\pm$ are separated by $2\nu_n$ and centered at $|A/2|$. For ^{14}N ($I = 1$), the $\nu_\pm$ branches are further split by the orientation-dependent quadrupole interaction, with the splitting denoted as 3P. Complete ^{1}H hyperfine tensors were derived from the frozen-solution samples through simulation of 2D field-frequency plots composed of multiple ENDOR spectra taken across the EPR envelope of the paramagnetic species under study, following published procedures.[31−34] The hyperfine tensor is defined by the principal tensor components, $[A_1, A_2, A_3]$, and the relative orientation of the tensor-frame with respect to g-frame, defined by Euler angles, $[\varphi, \theta, \psi]$.[35]

Computational Details. Density functional theory (DFT) calculations were performed using Amsterdam Density Functional (ADF) software with the BLYP functional in a spin-unrestricted formalism, and converged to ADF default criteria.[36] The TZ2P basis set with a small core potential was used for all atoms for geometry optimization calculations. The TZ2P basis set and no core potentials were used for calculations of hyperfine values. The initial model geometries were taken from crystal structures of the active sites of SOR[7] and CN-P450cam[15] (PDB ID 1DQI and 1O76, respectively). The axial-bonded oxygen of Glu14 in the SOR crystal structure was replaced with CN^-, the coordinating histidines were modeled with neutral imidazoles, and the axial Cys111 was shortened to $(SCH_2CH_3)^-$ to give a computational model structure of $[Fe(CN)(imidazole)_4(SCH_2CH_3)]^+$. The CN-P450cam geometry was similarly abbreviated as $[Fe(CN)(porphyrin)(SCH_2CH_3)]^-$.

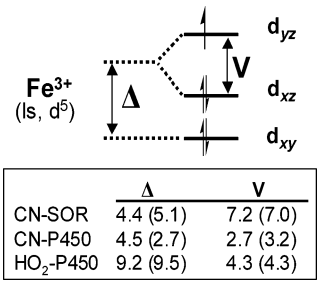

	Δ	V
CN-SOR	4.4 (5.1)	7.2 (7.0)
CN-P450	4.5 (2.7)	2.7 (3.2)
HO_2-P450	9.2 (9.5)	4.3 (4.3)

Figure 2. Crystal-field diagram of the low-spin d^5 CN-SOR and CN-P450 centers with tetragonal (Δ) and rhombic (V) splittings of the t_{2g} orbitals calculated from the expressions of Taylor, which assume the orbital reduction factor $k = 1$; slightly different values, shown in parentheses, are obtained if k is allowed to vary. Values are in units of the one-electron spin−orbit coupling constant, $\lambda \approx 400$ cm^{-1}.

Results

EPR Spectra. The cyano-ferric derivatives of SORs are low-spin ($S = {}^1/_2$) with a nearly axial **g** tensor and very small g-value anisotropy for low-spin Fe^{3+};[37,38] $g_{1,2,3} = [2.27, 2.24, 1.94]$ for *P. furiosus* 1Fe-SOR, based on simulations of Q-band EPR spectra.[24] Cyano-ferric-P450cam is also low-spin with larger g-value anisotropy, $g_{1,2,3} = [2.63, 2.28, 1.80]$. The well-known crystal-field treatment of a low-spin d^5 system can be used to analyze the observed g-values for these centers in terms of an interplay of spin−orbit coupling ($\lambda \approx 400$ cm^{-1} for a ferric site with significant covalent bonding) with tetragonal and rhombic crystal-field splittings of the t_{2g} dπ orbitals (Figure 2).[39] For a tetragonal distortion along z the axial splitting parameter, Δ, is defined as the difference between the average energy of the $[d_{xz}, d_{yz}]$ orbitals and the energy of the d_{xy} orbital. The rhombic splitting parameter, V, is the difference between the energies of the d_{xz} and d_{yz} orbitals.

Application of this analysis to the g-values for CN-P450cam gives the (Δ,V) pair listed in Figure 2. The tetragonal axis (z) is perpendicular to the heme plane, and the sign of Δ corresponds to an axial "elongation", meaning that the "crystal field strength" of the axial ligands is less than those of the in-plane pyrrole ligands. The unpaired electron is in an out-of-plane iron d_π orbital that is available for $d_\pi - p_\pi$ interaction with cysteinyl sulfur and the bound CN^-. This choice of axes, which corresponds to our "intuitive" views of a ferric-heme center also corresponds to the simplest (canonical) crystal-field description of the distortions, in which the crystal-field parameters obey the inequality $(V/\Delta) \leq 1$.

In contrast to CN-P450cam, analysis of the EPR, UV−visible absorption, CD, and VTMCD spectra of the cyanide-bound ferric SOR site in *P. furisosus* 1Fe-SOR showed that the canonical treatment of its electronic structure corresponds to octahedral coordination geometry with the largest (tetragonal) elongation along an in-plane axis that connects *trans*-histidyl nitrogens and an out-of-plane rhombic distortion. Thus, the crystal-field strength of that pair of histidines is less than the average strength of the other two histidines and the axial cyanide

(28) Sono, M.; Dawson, J. H. *J. Biol. Chem.* **1982**, *257*, 5496−5502.
(29) Davoust, C. E.; Doan, P. E.; Hoffman, B. M. *J. Magn. Reson.* **1996**, *119*, 38−44.
(30) Yang, T.-C.; Hoffman, B. M. *J. Magn. Reson.* **2006**, *181*, 280−286.
(31) Hoffman, B. M.; Martinsen, J.; Venters, R. A. *J. Magn. Reson.* **1984**, *59*, 110−123.
(32) Hoffman, B. M.; Venters, R. A.; Martinsen, J. *J. Magn. Reson.* **1985**, *62*, 537−542.
(33) Hoffman, B. M.; DeRose, V. J.; Doan, P. E.; Gurbiel, R. J.; Houseman, A. L. P.; Telser, J. *Biol. Magn. Reson.* **1993**, *13(EMR of Paramagnetic Molecules)*, 151−218.
(34) Doan, P. E. In *Paramagnetic Resonance of Metallobiomolecules*; Telser, J., Ed.; American Chemical Society: Washington D.C., 2003; pp 55−81.
(35) Mathews, J.; Walker, R. L. *Mathematical Methods of Physics*; W. A. Benjamin, Inc.: New York, 1965.
(36) ADF version 2005.01, SCM, Theoretical Chemistry, Vrije Universiteit, Amsterdam, The Netherlands, http://www.scm.com.
(37) McGarvey, B. R. *Coord. Chem. Rev.* **1998**, *170*, 75−92.
(38) Peisach, J.; Blumberg, W. E.; Adler, A. *Ann. N.Y. Acad. Sci.* **1973**, *206*, 310−327.
(39) Taylor, C. P. S. *Biochim. Biophys. Acta* **1977**, *491*, 137−149.

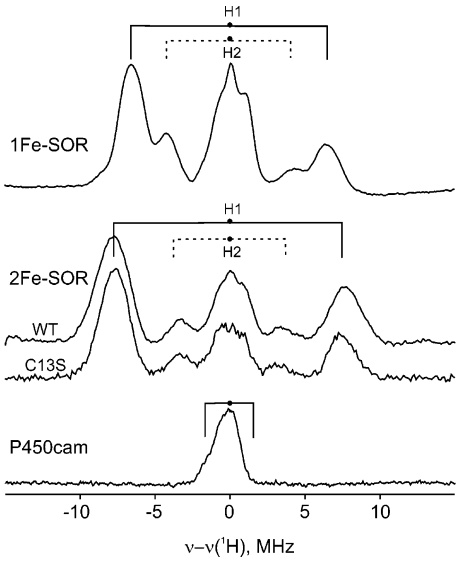

Figure 3. ^{1}H Q-band CW ENDOR spectra collected at g_1 for CN-1Fe-SOR, WT and C13S CN-2Fe-SOR, and CN-P450cam. *Experimental conditions*: mw frequencies = 34.96−35.08 GHz; mw power = 30 μW; modulation = 4 G; RF scanning speed = 1 MHz/s; bandwidth broadening = 100 kHz.

and thiolate ligands. However, as with CN-P450cam, the unpaired electron is in an out-of-plane iron d_π orbital that is available for $d_\pi-p_\pi$ interaction with axial ligands.[13] Because the odd-electron d_π orbitals in CN-P450cam and CN-SOR have equivalent spatial orientations, to facilitate comparison between them, it is appropriate to likewise analyze the CN-SOR *g*-values in terms of an out-of-plane tetragonal distortion, even though this is not a canonical description and gives crystal-field parameters (Δ, V; Figure 2) which have the relationship, $V/\Delta > 1$. By doing so, the tetragonal parameter for both enzymes corresponds to a difference between crystal-field strengths of the axial (cyanide and thiolate) and equatorial (N_4) ligands.

For both enzymes, the tetragonal parameter, Δ, corresponds to an axial "elongation" and within the precision of this treatment Δ is essentially the same for both centers, $\Delta = 4.4-4.5$. This implies that the *average* "crystal-field" strengths of the equatorial N_4 ligand sets in the two enzymes (four pyrrole N of the CN-P450cam heme and four His N in CN-SOR) are essentially the same. In contrast, the rhombic splitting parameter, V, is more than twice as large for CN-SOR than for CN-P450cam. The large rhombic distortion clearly reflects the large variations in the dihedral angles of the histidyl ligands, which introduces a strong *effective* in-plane distortion and accompanying d_π splitting that likely has little to do with actual π bonding.

The putative hydroperoxo-ferri-SOR, which is the alleged active intermediate has not been trapped for EPR study. However, the *g*-values for hydroperoxo-ferri-P450cam have been measured, $g = [2.29, 2.17, 1.96]$. These correspond to a tetragonal crystal-field parameter of $\Delta = 9.2$, which is twice that calculated for CN-P450cam and CN-SOR. As this parameter corresponds to an axial elongation, the larger value of Δ unsurprisingly indicates that $[OOH]^-$ is a much weaker ligand than $[CN]^-$. The rhombic splitting parameter of hydroperoxo-ferri-P450cam, ($V = 4.3$) is noticeably larger than that for CN-P450cam, an increase which reflects the influence of π bonding to and/or bending of the $[OOH^-]$ ligand.

Cysteine Axial Ligand. CW ^{1}H ENDOR Spectra at g_1. Figure 3 shows CW ^{1}H ENDOR spectra taken at g_1 for the [Fe-

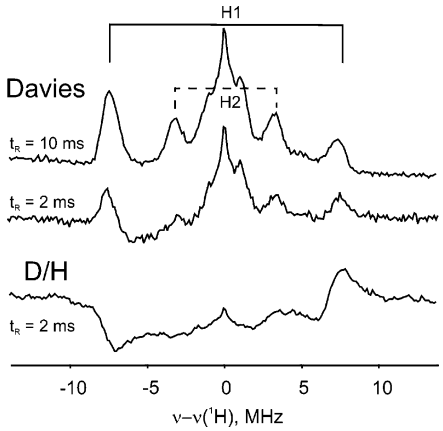

Figure 4. ^{1}H ENDOR spectra taken at g_1 for CN-1Fe-SOR collected with the modified Davies/Hahn spin−echo ENDOR pulse sequence (repetition time, $\tau_R = 2$ ms) and Davies spin−echo (pulsed) ENDOR spectra collected with $\tau_R = 2$ and 10 ms, respectively. *Experimental conditions*: $\pi/2 = 40$ ns; RF = 100 μs with 100 kHz bandwidth broadening; resolution = 256 points; data average = 2000 transients/point; $T = 2$ K.

$(NHis)_4(SCys)(CN)$] centers of oxidized WT *P. furiosus* 1Fe-SOR and WT and C13S *D. vulgaris* 2Fe-SOR. The ^{1}H spectra are comprised of $\nu_\pm$ doublets, centered at the proton Larmor frequencies and split by the hyperfine coupling, *A*. Each of the SORs shows two strongly coupled doublets. At this field, the larger of the two proton couplings (A(H1)) for the 1Fe-SOR is ~15 MHz, the smaller (A(H2)) is ~8 MHz; A(H1) is slightly greater, ~17 MHz, for the WT and C13S 2Fe-SOR. These ^{1}H signals are not lost when the enzymes are exchanged into D_2O solvent, and couplings to histidyl protons are small.[40,41] Hence, these large couplings are assigned to the two inequivalent methylene β protons of the cysteinyl axial ligand. In addition, for all three CN-SORs investigated, there is a poorly resolved feature centered at the Larmor frequency, breadth ~3−4 MHz, associated with more weakly coupled protons, plausibly those of the in-plane histidines.

In contrast, the ^{1}H ENDOR spectrum taken at g_1 for cyano-ferric-P450cam in D_2O buffer, also shown in Figure 3, has no strongly coupled proton signals, instead showing a narrow feature with a shoulder on the low-frequency side that likely corresponds to the ν_- feature of a proton signal with $A \approx 3$ MHz; the ν_+ partner has negligible intensity. This spectrum is similar to that previously reported for aquo-ferric-P450cam.[42,43] Hence, the cysteinyl β protons of both low-spin ferric-P450cam forms have couplings ≤ 3 MHz. Similar results were obtained for hydroperoxo-ferri-P450cam, both with and without bound camphor.[9]

Determination of the Sign of Cysteinyl β-^{1}H Hyperfine Couplings. The ^{1}H CW ENDOR spectra of CN-SORs at g_1 are unlike most collected at 35 GHz, in that the ν_- peaks have greater intensities than the ν_+ peaks. This behavior also is seen in the ^{1}H Davies spin−echo (pulsed) ENDOR spectrum of Figure 4. The relative intensities of the ν_+ and ν_- branches are governed by an interplay between the operative electron spin

(40) Scholes, C. P.; Falkowski, K. M.; Chen, S.; Bank, J. *J. Am. Chem. Soc.* **1986**, *108*, 1660−1671.
(41) Scholes, C. P.; Lapidot, A.; Mascarenhas, R.; Inubushi, T.; Isaacson, R. A.; Feher, G. *J. Am. Chem. Soc.* **1982**, *104*, 2724−2735.
(42) Davydov, R.; Macdonald, I. D. G.; Makris, T. M.; Sligar, S. G.; Hoffman, B. M. *J. Am. Chem. Soc.* **1999**, *121*, 10654−10655.
(43) LoBrutto, R.; Scholes, C. P.; Wagner, G. C.; Gunsalus, I. C.; Debrunner, P. G. *J. Am. Chem. Soc.* **1980**, *102*, 1167−1170.

relaxation mechanisms and the Boltzmann populations of the electron spin states as transferred among the electron-nuclear spin levels by ENDOR transitions.[30,44] Analysis of the peak intensities and phases as monitored with the modified Davies/Hahn (D/H) spin−echo ENDOR multipulse sequence allows us to determine the absolute signs of the hyperfine couplings. A simple electron-nuclear spin-relaxation model[30] for [$S = {}^1/_2$, $I = {}^1/_2$] shows that the ENDOR peak(s) in a D/H spectrum that are associated with the electron spin $M_S = -{}^1/_2$ substate always have a positive phase, defined as an ENDOR-induced increase in the electron spin−echo intensity. The ENDOR transitions associated with the $M_S = +{}^1/_2$ substate should have an algebraically smaller intensity, but the intensity is not always reliable when the phase is positive, as it can be influenced by other factors such as frequency dependence of the RF power. However, the phase of the $M_S = +{}^1/_2$ signals can become negative under favorable combinations of the repetition time, τ_R, the electron-spin relaxation time, T_{1e}, and cross relaxation. Such a phase inversion is a robust signature of $M_S = +1/2$ nuclear transitions.

Figure 4 shows the ^{1}H pulsed ENDOR spectrum of the 1Fe-SOR collected at g_1 with the ordinary Davies sequence at two different values of the repetition time and with the D/H multi-sequence at the shorter repetition time (2 ms). The ν_- branch of the H1 doublet is more intense in the Davies spectra taken with both repetition times. However, the ν_+ branch retains a positive phase in the H/D spectrum collected at $\tau_R = 2$ ms, whereas the ν_- branch inverts. This finding unambiguously indicates that ν_+, which has positive phase in all spectra, is the $M_S = -1/2$ transition for H1, and this implies that A(H1) is positive. The absolute sign for the coupling to the other β proton, A(H2), is the same as that for A(H1), and the τ_R dependence of the spectra support this, although the inverted phase in the ν_- branch is not as clear as that for A(H1) because the pulse selectivity is less for the smaller hyperfine coupling.

As discussed below (eq 2), A(H) for a cysteinyl β proton has the same sign as the spin density on sulfur, ρ_s. The positive sign of the hyperfine couplings for the CN-SOR H_β protons thus implies that $\rho_s > 0$; the same result is obtained for the C13S mutant of 2Fe-SOR (data not shown). These experiments fail with the WT 2Fe-SOR because the electron-spin relaxation is too fast, presumably because of spin−spin interactions between the [$Fe(N_{His})_4(S_{Cys})$] and the [$Fe(S_{Cys})_4$] centers. However, we assign the same positive sign to the β-proton hyperfine couplings and the sulfur spin density for both 1Fe-SOR and 2Fe-SOR, on the basis of the close similarity of their CN-SOR sites.

With the putative proton signals from the cysteinyl β proton(s) of CN-P450cam so poorly resolved, it is not possible to measure the sign of the sulfur spin density similarly. However, it is certainly the same as for CN-SOR, $\rho_s > 0$.

Orientation-Selective 2D CW ^{1}H-ENDOR Spectra of SORs. Figure 5 shows the 2D ^{1}H ENDOR pattern for 1Fe-SOR; similar patterns were collected for all other CN-SORs investigated (data not shown). The features for the methylene protons, H1 and H2, can be followed throughout the pattern; those for H1 are quite clearly discerned, whereas those for H2, indicated by the dotted lines, are less so. The ν_+ peaks split

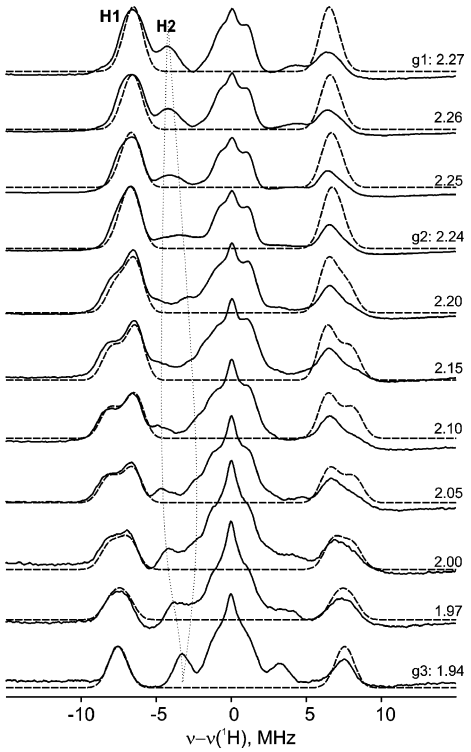

Figure 5. Orientation-selective Q-band CW ^{1}H ENDOR experimental and simulated spectra for CN-1Fe-SOR. The conditions are as in Figure 3. *Simulation parameters*: EPR line width = 500 MHz; **(H1)**: A = [12.5, 12.5, 17.0] MHz; Euler angles = [70°, 40°, 20°]; ENDOR line width = 1.3 MHz; **(H2)**: A = [7.0, 11.0, 5.0] MHz; Euler angles = [10°, 30°, 80°]; ENDOR line width = 1.0 MHz.

and coalesce again as the field is increased from g_1 to g_3, but the center of gravity of each ν_+/ν_- feature for both protons shifts little, indicating that the hyperfine coupling for both are dominated by the isotropic coupling, a_{iso}(H). This is expected for β-proton couplings generated by hyperconjugation with spin in a p_π orbital on the cysteinyl sulfur. The figure includes excellent simulations of the H1 features (dashed lines) as calculated from the hyperfine tensors listed in Table 1, along with the similar parameters for the other CN-SORs. Because the H2 peaks are less well resolved, precise fitting is difficult, and simulations are not shown. However, the isotropic component for H2 is well defined for all three CN-SORs, and values are also listed in Table 1. The large a_{iso}(H) are indicative of the strong covalent interaction between iron d_π and the sulfur p_π orbitals of SOR, as first established by UV−visible absorption/VTMCD and resonance Raman studies of *P. furiosus* 1Fe-SOR.[20,45] The β-protons also show a small anisotropic interaction, and values for this are listed in Table 1.

Experimental Spin Density on the Cysteinyl Sulfur of CN-SOR. The isotropic hyperfine couplings for β-protons of a cysteinyl ligand to an $S = {}^1/_2$ metal ion are proportional to ρ_s, the spin density in the cysteinyl sulfur π orbital, oriented perpendicular to the Fe−S−C_β plane,[21,22,46,47] such that

$$A_{iso}(H) = B\rho_s[\cos^2\theta] \qquad (2a)$$

where the coupling parameter B has been estimated to be ∼+80−100 MHz (see below), and θ is the dihedral angle

(44) Epel, B.; Poppl, A.; Manikandan, P.; Vega, S.; Goldfarb, D. *J. Magn. Reson.* **2001**, *148*, 388−397.

(45) Clay, M. D.; Jenney, F. E., Jr.; Noh, H. J.; Hagedoorn, P. L.; Adams, M. W. W.; Johnson, M. K. *Biochemistry* **2002**, *41*, 9833−9841.

Table 1. ENDOR-Determined Hyperfine Coupling Parameters of the Cysteinyl $^1H_\beta$ and Cyano ^{13}C Atoms in CN-SORs and CN-P450cam

	a_{iso} (MHz)	A_{aniso} (MHz)	angle[a] (deg)	$B\rho_S$ (MHz)
		1Fe-SOR WT		
H1	14.0	[−1.5, −1.5, 3.0]	−74 (−84)[b]	15.1
H2	7.7	[−0.7, 3.3, −2.7]	46 (36)[b]	
C1	−32.8	[−1.2, −1.2, 2.4]	175	
C2	−26.7	[−0.3, −0.3, 0.6]	133	
C3	−23.2	[0.2, 3.2, −3.4]	123	
		2Fe-SOR WT		
H1	16.8	[−1.8, 1.2, 0.7]	−78 (−84)[b]	17.5
H2	7.7	[−0.7, −0.7, 1.3]	42 (42)[b]	
C1	−31.2	[−0.8, −0.8, 1.6]	175	
C2	−25.3	[0.3, 0.3, −0.6]	133	
C3	−22.3	[1.3, 1.3, −2.6]	124	
		C13S 2Fe-SOR		
H1	16.0	[−2.0, 1.0, 1.0]	−77 (−84)[b]	16.8
H2	7.7	[−0.7, −0.7, 1.3]	43 (42)[b]	
C1	−31.2	[−1.3, −0.3, 1.6]	175	
C2	−25.0	[0.0, 1.0, −1.0]	132	
C3	−22.0	[1.0, 2.0, −3.0]	123	
		P450cam		
H1/2	<3	−	(−30,−149)[b]	<14
C1	−21.5	[−4.5, 2.9, 1.5]	119	

[a] Indicates Fe−S−C_β−H dihedral for H and Fe−C−N bend for C. [b] Analogous angle obtained from X-ray crystal structure.

between the sulfur p_π orbital and the C_β−H bond.[48] eq 2a can be rewritten for convenience as

$$a_{iso}(H) = B\rho_s[\sin^2\theta'] \quad (2b)$$

where θ' is the Fe−S−C_β−H dihedral angle. If the dihedral angle for the H1 methylene proton is denoted as θ'_1, then the dihedral angle for H2 is $\theta_2' = \theta'_1 \pm 120°$ for ideal tetrahedral hybridization at C_β. Through use of the two measured isotropic couplings a_{iso}(H1, H2), eq 2b can be solved for each SOR to give values for θ_1' and $B\rho_s$, and these are listed in Table 1. The crystallographic Fe−S−C_β−C_α dihedral angles for oxidized *P. furiosus* 1Fe-SOR and *D. desulfuricans* 2Fe-SOR (156° and 162° respectively)[7,8] correspond to the Fe−S−C_β−H dihedral angles (θ_1', θ_2') given in Table 1 for 1Fe-SOR and 2Fe-SOR. They are within ∼ 10° of the ENDOR values for 1Fe-SOR, while they match precisely for the 2Fe-SORs. Indeed, the small deviation for the 1Fe-SOR may merely reflect the fact that a_{iso}(H) falls in a region where significant changes in the ratio cause only small variation on θ_1' and θ_2'. The resulting spin density in the π orbital of sulfur is $\rho_s \approx 0.20/0.17$ for the CN-SORs investigated in this work, with the higher value corresponding to $B = +83$ MHz, as determined from an RCH_2S radical similar to the cysteine ligand,[49] and the lower value corresponding to $B = +100$ MHz, as suggested by Gordy.[46,50]

(46) Gordy, W. *Theory and Applications of Electron Spin Resonance*; John Wiley & Sons: New York, 1980.
(47) Epel, B.; Slutter, C. S.; Neese, F.; Kroneck, P. M. H.; Zumft, W. G.; Pecht, I.; Farver, O.; Lu, Y.; Goldfarb, D. *J. Am. Chem. Soc.* **2002**, *124*, 8152−8162.
(48) In this equation, an additional small angle-independent contribution to the coupling parameter has been ignored.
(49) Akasaka, K.; Ohnishi, S.; Suita, T.; Nitta, I. *J. Chem. Phys.* **1964**, *40*, 3110−3116.
(50) For completeness, we note that eq 2b has a second solution for CN-1Fe-SOR that yields ($\theta_1' = 35°$, $\theta_2' = 155°$) and $B\rho_s = 42.5$ MHz, a value close to that seen for blue-copper centers. However, the dihedral angles obtained with this solution are far from those obtained from X-ray crystallographic structure of SORs. Moreover, for coplanar iron, sulfur, C_β, C_α atoms, $\theta_1' = \theta_2' = -60°$, which predicts equal couplings for each of the two β protons, contrary to our observations.

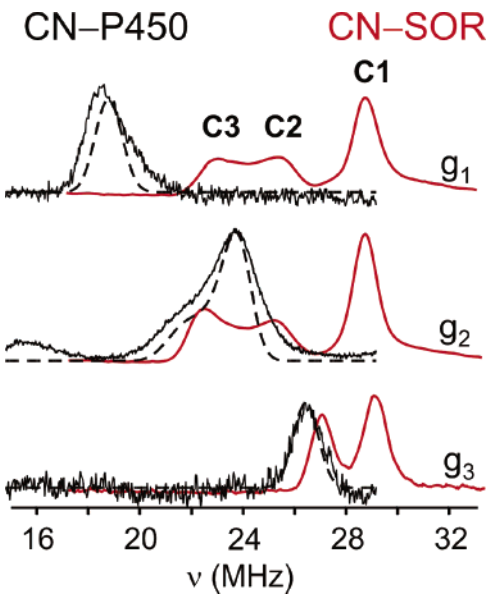

Figure 6. CW ^{13}C ENDOR spectra of CN-1Fe-SOR and CN-P450cam collected at the three canonical g values. The dashed lines are simulated spectra generated with the following parameters: EPR line width = 400 MHz; ENDOR line width = 1.1 MHz; **A** = [17.0, 24.4, 23.0] MHz; Euler angles = [0°, 5°, 10°]. *Experimental conditions:* 35.07 GHz; mw power = 30 μW; 100 kHz modulation amplitude = 4 G; RF scanning speed = 1.0 MHz/s; bandwidth broadening = 100 kHz.

Table 1 also lists the parameters describing the small anisotropic contribution to the proton couplings. In all three cases, these can be described by an axial (dipolar) interaction where the single defining parameter is $T \approx 1$ MHz. The observed dipolar term may be assigned to a through-space dipolar interaction with the spin on sulfur. For such a nonlocal dipolar interaction, $T_{nl} = \rho_S g_e \beta_e g_n \beta_n / r^3$, where ρ_S again is the unpaired spin density on sulfur, r is the S−H distance, and the other parameters have their conventional meanings. Since T_{nl} decreases with distance as r^{-3}, the additional coupling term to the spin on the ferric iron center is negligible. Taking $\rho_S = 0.20$ gives $r \approx 2.2$ Å, adequately near the distance between H_β and sulfur in cysteine (∼2.46 Å), which indicates that this interaction is the main source of the coupling; more detailed analysis is not warranted.

Experimental Spin Density on the Cysteinyl Sulfur of CN-P450cam. We have provisionally assigned the largest ^1H coupling for CN-P450cam, $A \approx 3$ MHz, to the cysteinyl β-protons and have assumed a small anisotropic contribution to the hyperfine tensor for these nuclei. This may be taken as a value for a_{iso}(H1). The average Fe−S−C_β−C_α dihedral angle for the two independent CN-P450cam sites is 91°, which corresponds to (θ_1', θ_2') = (−30°, −149°) for the cysteinyl methylene protons. Insertion of these angles, along with a_{iso}(H1) ≈ 3 MHz, into eq 2b with $B = 83$ MHz, gives $\rho_s \approx 0.14$ as the upper limit of the spin density in the π orbital of the coordinated sulfur of CN-P450cam. Thus, the spin density on sulfur in CN-P450cam is only slightly less (∼2/3) than that in CN-SOR, despite the 5-fold difference (or greater) in ^1H hyperfine couplings.

Cyanide Axial Ligand. Experimental Results for CN^- Axial Ligand. Figure 6 presents ^{13}C ENDOR spectra of cyano-ferric-1Fe-SOR and cyano-ferric-P450cam collected at the three canonical g values of each. The g_1 spectrum of CN-SOR shows three ν_+ peaks associated with three CN substates (C1−C3).

The differing variation in peak frequencies with g-value for the different substates reflects an interplay between the intrinsic hyperfine anisotropy, as altered by bending of the Fe−C−N linkage, and a change in the *effective* hyperfine coupling with the g-value of observation (g_{obs}), which is roughly proportional to (g_{obs}/g_e). Full field dependences have been published for this and the other CN-SORs investigated in this work, and the hyperfine tensors derived from these data are recalled in Table 1.[24]

The single feature at g_1 for CN-P450cam shows that this enzyme has a single Fe−C−N substate. The field dependence of the ^{13}C ENDOR frequencies is greater than those for CN-SOR and the analysis of the 2D field-frequency plot (in Supporting Information) gives the hyperfine tensor **A** (Table 1), which has an isotropic hyperfine value $a_{iso} = -21.5$ MHz (sign determined as previously). As with SOR, A_1 lies along g_1 (heme normal), but for CN-P450cam, A_2 and A_3 are rotated slightly ($\varphi = 5°$) relative to g_1 and g_2.

The isotropic ^{13}CN couplings are associated with *s*-orbital spin density in the sp^n hybrid orbital on carbon that participates in the Fe−C bond. The magnitude of the isotropic coupling, $|a_{iso}|$, *decreases* from CN-SOR substate 1 → 3 while the contribution to the dipolar parameter, T, that comes from p spin density in the sp^n hybrid orbital on carbon *increases*. We used a simple heuristic ("rigid-orbital") bonding model to explain these synchronous, but opposing, changes in terms of a progressive decrease in the Fe−C−N angle, θ, and corresponding increase in n of the sp^n hybrid, and used this model to attain estimates of θ. According to this model, the spin density in the bonding hybrid orbital remains constant as θ decreases, while the ratio of $a_{iso}(\theta)$ to the value for linear Fe−C−N ($\theta = \pi$) varies with θ because of changes in hybridization of the sp^n orbital on carbon that binds to the iron according to the simple function,

$$\frac{a_{iso}(\theta)}{a_{iso}(\pi)} = \frac{\cos(\theta)}{[\cos(\theta) - 1]} \qquad (3)$$

Taking $\theta = 175°$ for the C1 substate of SOR, based on vibrational spectroscopy,[24] gave $\theta = 133°$ and 123° for C2 and C3, respectively. *If* $a_{iso}(\pi)$ for CN-SOR and CN-P450cam were equal, then $a_{iso} = -21.5$ MHz for CN-P450cam would correspond to $\theta = 119°$, a slightly greater bend even than in substate C3 of CN-SOR. The variation of a_{iso} with θ in the two enzymes is discussed in more detail below where we report DFT computations. We note here that one conclusion of these computations is that this "rigid-orbital" model likely underestimates θ (overestimates bending) for large deviations from linearity, $\theta \lesssim 140°$, a conclusion that is supported by the crystallographically defined Fe−C−N angles of 138° and 152° in camphor-bound cyano-ferric-P450cam.[15] Near-room-temperature solution resonance Raman data for CN-P450cam found both linear and bent forms, both in the absence and presence of camphor. Comparison implies that the linear form observed in solution is converted to the bent form in frozen solution and the crystalline state.[25,26]

Equatorial Nitrogen Ligands. ^{14}N CW ENDOR of Equatorial Ligands. Figure 7 shows the ^{14}N ENDOR spectrum for CN-1Fe-SOR taken at g_1; CN-2Fe-SOR gives similar spectra (not shown). As indicated, the spectrum with the field along g_1 contains ν_+ features from the four bound histidyl nitrogens, each with a further splitting into a doublet by the ^{14}N quadrupole interaction denoted as $3P_{11}'$. Two-dimensional (2D) field-frequency plots comprised of spectra collected at fields across the EPR envelope indicate that the hyperfine couplings are roughly isotropic, as expected from earlier work,[41] but it is impractical to derive the full ^{14}N hyperfine and quadrupole tensors for the four ^{14}N from such overlapping patterns. Nonetheless, and perhaps surprisingly, it is possible to assign the ^{14}N spectrum at the g_1 single-crystal-like orientation uniquely to the four crystallographically visualized histidines. *First*, we know the quadrupole coupling tensor for an N_{His} bound to ferric iron, $\mathbf{P} = [P_{11}, P_{22}, P_{33}] = [0.31, 0.81, -1.12]$ MHz,[41] where the P_{33} quadrupole axis lies along the Fe−N bond and P_{11} lies normal to the imidazole ring. *Second*, as shown in our recent study,[24] the g_1 axis of the CN-SOR is normal to the plane containing the four Fe−N_{His} bonds. As a result, in a CN-SOR ^{14}N ENDOR spectrum taken at g_1, the external field is normal to the four Fe−N bonds, and the quadrupole splitting is a simple function of P_{11}, P_{22}, and the dihedral angle β, by which the histidine plane is rotated about the Fe−N_{His} bond out of the plane normal to g_1:

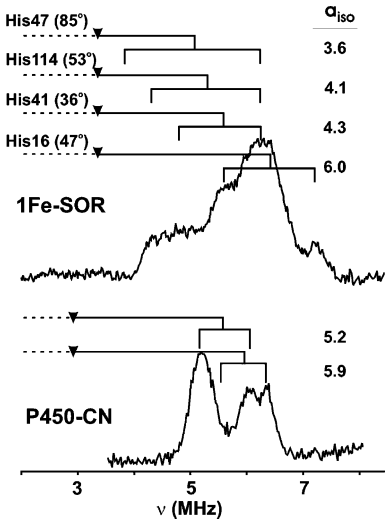

Figure 7. CW ^{14}N ENDOR spectra collected at g_1 for CN-1Fe-SOR and CN-P450cam. *Experimental conditions*: 35.03−35.11 GHz; mw power = 30 μW; 100 kHz modulation amplitude = 4 G; RF scanning speed = 0.25 MHz/s; bandwidth broadening = 25 kHz.

$$3P_{11}' = 3(P_{11}\cdot\cos^2\beta + P_{22}\cdot\sin^2\beta) \qquad (4)$$

The X-ray structure of the ferric 1Fe-SOR yields the dihedral β angles of the four histidine rings: 47° (His16), 36° (His 41), 85° (His47), 53° (His114).[7] With all parameters needed to apply eq 4 available for each N(His), we have calculated the $3P_{11}'$ for each and assigned four quadrupole-split ν_+ doublets for the pattern of Figure 7. This match is not unique, but all reasonable assignments give comparable values for the hyperfine couplings along g_1 (A_{11}') which is dominated by the isotropic term. The resulting assignment in the figure gives an average value of $A_{11}' \approx a_{iso} = 4.5$ MHz, with a considerable *fractional* variation in the coupling: $A_{11}' \approx a_{iso} = 6.0$ (His16), 4.3 (His 41), 3.6 (His47), and 4.1 MHz (His114).[51]

(51) We note explicitly that the above discussion assumes that there is no variation of the ^{14}N hyperfine and quadrupole coupling parameters among the different substates disclosed by the ^{13}C ENDOR measurements.

Table 2. Selected Bond Lengths (Å) and Angles (deg) from DFT Optimization Calculations of CN-SOR and CN-P450 Active-Site Models[a]

calculation	Fe–N_{eq}	Fe–S	Fe–C	C–N	Fe–C–N	C_β–S–Fe–N1	C_α–C_β–S–Fe	θ'_1	θ'_2
				CN−SOR					
optimization of only CN	**2.16**	**2.46**	1.96	1.17	177	**11**	**156**	**−83**	**35**
optimization of all atoms	2.06	2.28	1.98	1.17	177	10	157	−83	34
optimization with $C_\alpha-C_\beta-S-Fe = 91°$	2.06	2.28	1.98	1.17	178	15	**91**	−150	−35
				CN-P450					
optimization of only CN	**2.01**	**2.39**	1.99	1.18	179	**4**	**91**	**−149**	**−30**
optimization of all atoms	2.03	2.34	2.00	1.17	179	0	100	−140	−24
optimization with $C_\alpha-C_\beta-S-Fe = 156°$	2.00	2.34	2.00	1.17	179	6	**156**	−82	34

[a] Values in bold type were constrained during optimization.

Figure 7 presents the ν_+ branch of the g_1 spectrum of the ^{14}N-pyrrole of CN-P450cam. As is typical in spectra of ferric hemoproteins, reduction in symmetry of the heme from its idealized four-fold symmetry causes the ν_+ branch to exhibit signals from two types of ^{14}N-pyrrole.[52] The quadrupole coupling tensor for an ^{14}N-pyrrole has been measured in a single-crystal study of ferric-Mb as $\mathbf{P} = [-0.77, 1.04, -0.27]$ MHz.[41] For CN-P450cam, g_1 again lies normal to the N_4 porphyrin plane, and this corresponds to the P_{33} quadrupole direction; thus, $\beta = 0°$ for the pyrroles, and one expects $3P_{33}' = 3P_{33}(-0.81)$ MHz. Assuming approximately such a quadrupole splitting, the CN-P450cam spectrum can be assigned as shown in Figure 7 to give $a_{iso} = 5.2$ and 5.9 MHz for the two types of ^{14}N-pyrrole. The average hyperfine coupling for the four N(His) of CN-1Fe-SOR, $a_{iso} = 4.5$ MHz, is significantly less than that of the average for CN-P450cam of $a_{iso} = 5.6$ MHz. In both cases, the hyperfine coupling for nitrogen bound to the low-spin ferric ion is thought to be induced by polarization of the Fe−N σ bond.

^{14}N ENDOR has been reported for hydroperoxo-ferri-P450cam, both with and without substrate bound.[42] Substrate-free hydroperoxo-ferri-P450cam gives $a_{iso} = 6.9$ and 5.6 MHz for the two types of ^{14}N-pyrrole. Inclusion of the camphor substrate causes a decrease in the coupling such that $a_{iso} = 6.4$ and 5.1 MHz for the two types of ^{14}N-pyrrole, only ∼0.2 MHz greater than the average for CN-P450cam.

DFT Computations. For further insights into the differences in the electronic characteristics of the $[Fe^{III}(CN)N_4S_{Cys}]$ coordination spheres of CN-SOR and CN-P450cam, DFT calculations comparing important coordination geometry differences, spin densities, and hyperfine values were performed. *First*, a series of geometry optimizations were performed for computational models of both active sites, starting from the crystal structures. Some of these include specific constraints in order to test the robustness of the calculated bonding description. A summary of selected bond lengths and angles is shown in Table 2, and the corresponding atom labeling scheme is shown in Figure 8. *Second*, to identify the geometric parameters that most influence hyperfine values, two additional series of optimizations with constrained Fe−S−C_β−C_α and Fe−C−N angles were carried out. *Third*, we modeled the influence of H-bonding to cysteinyl sulfur by use of fractional static point charges at the positions of the H-bonding protons. Complete tables of the calculation results are available in Supporting Information.

Active-Site Models Geometry Optimizations. The fully optimized geometry of the CN-SOR model had Fe−N and Fe−S bond lengths ∼0.1 Å and ∼0.2 Å shorter than the crystal

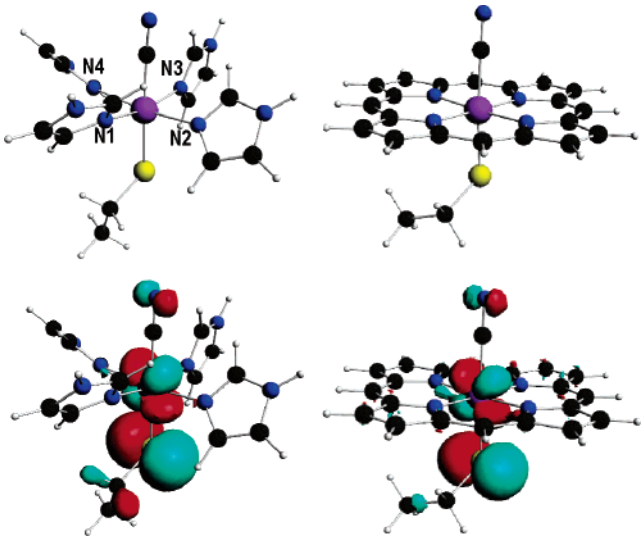

Figure 8. (Top) Computational model structures used for the DFT calculations showing the numbering positions of the equatorial nitrogen atoms. The atom numbering is analogous to that for the CN-P450 model. (Bottom) Molecular orbital contour plot of the HOMOs resulting from all-atom DFT optimizations of the models.

structure values, respectively. Such shortening often is observed for DFT optimizations of transition metal complexes. Partial geometry optimizations were done to test the significance of the short Fe−N and Fe−S bond lengths and the orientations of the imidazole rings. In all these optimizations, Fe−C−N remained nearly linear and the Fe−C and C−N bond lengths were reasonable. When the dihedral angles of the imidazole rings relative to the Fe−N_4 plane were allowed to vary, the crystal structure values were retained within ± 15°. Moreover, the optimized geometry of the cysteinyl sulfur ligand remained similar to that of the crystal structure where the N1−Fe−S−C_β dihedral angle is ∼15° and the Fe−S−C_β−C_α dihedral angle is ∼160°.

For the CN-P450 model, the optimized average equatorial Fe−N bond length is very similar to the average crystal structure value, likely as a result of the greater rigidity of the porphyrin compared to that of the histidine ligands of CN-SOR. The optimized Fe−S bond length is again short but only by ∼0.05Å. The axial Fe−C−N angle optimizes to nearly linear in all cases, unlike the ∼145° bend observed in the crystal structure, although the experimentally observed bend is believed to arise from hydrogen bonding to the cyano nitrogen that is not present in our model.[15] Interestingly, like the CN-SOR calculations, the optimized thiolate ligand geometry again displays dihedral angles consistently similar to those of the crystal structure values, where the N1−Fe−S−C_β dihedral angle is ∼5° and the Fe−S−C_β−C_α dihedral angle is ∼90° for CN-P450. Further-

(52) Davydov, R.; Perera, R.; Jin, S.; Yang, T.-C.; Bryson, T. A.; Sono, M.; Dawson, J. H.; Hoffman, B. M. *J. Am. Chem. Soc.* **2005**, *127*, 1403−1413.

Table 3. Spin Densities Resulting from DFT Calculations of CN-SOR and CN-P450 Active-Site Models

calculation parameters	Fe	S	N_{eq}	C_{CN}	H1	H2
CN-SOR						
optimization of only CN	0.643	0.371	−0.008	−0.029	0.013	0.004
optimization of all atoms	0.695	0.322	−0.009	−0.029	0.013	0.004
optimization with Fe−C−N = 180°	0.689	0.325	−0.009	−0.028	0.013	0.004
optimization with Fe−C−N = 120°	0.768	0.259	−0.010	−0.010	0.008	0.007
Fe−C−N = 180° + two 0.2 pt ch	0.771	0.250	−0.011	−0.032	0.010	0.003
Fe−C−N = 120° + two 0.2 pt ch	0.834	0.201	−0.012	−0.012	0.007	0.005
CN-P450						
optimization of only CN	0.753	0.306	−0.009	−0.031	0.002	0.005
optimization of all atoms	0.766	0.309	−0.009	−0.031	0.004	0.002
optimization with Fe−C−N = 180°	0.769	0.307	−0.009	−0.031	0.004	0.002
optimization with Fe−C−N = 120°	0.839	0.241	−0.010	−0.006	0.004	0.000
Fe−C−N = 180° + three 0.2 pt ch	0.869	0.184	−0.011	−0.036	0.002	0.001
Fe−C−N = 120° + three 0.2 pt ch	0.908	0.147	−0.012	−0.003	0.002	0.000

Table 4. Isotropic Hyperfine Values (MHz) from DFT Calculations of CN-SOR and CN-P450 Active-Site Models

calculation parameters	N1	N2	N3	N4	C_{CN}	H1	H2
CN-SOR							
optimization of only CN	−4.8	−1.7	−2.9	−1.1	−19.4	48.2	23.6
optimization of all atoms	−4.3	−1.3	−3.8	−2.0	−17.8	34.1	12.6
optimization with Fe−C−N = 180°	−4.3	−1.0	−3.7	−2.0	−17.9	34.1	15.6
optimization with Fe−C−N = 120°	−4.9	−3.0	−4.1	−3.1	−9.2	23.7	19.7
Fe−C−N=180° + two 0.2 pt ch	−4.9	−2.1	−4.2	−3.2	−20.1	28.8	9.9
Fe−C−N=120° + two 0.2 pt ch	−5.5	−3.6	−4.5	−3.9	−11.8	19.6	14.8
CN-P450							
optimization of only CN	−4.3	−1.6	−4.4	−2.9	−21.4	9.2	4.8
optimization of all atoms	−4.4	−1.8	−4.3	−1.7	−21.8	10.8	2.4
optimization with Fe−C−N = 180°	−4.4	−1.7	−4.4	−1.9	−21.8	10.5	2.4
optimization with Fe−C−N = 120°	−4.9	−3.4	−4.7	−2.8	−7.3	10.5	−0.4
Fe−C−N=180° + three 0.2 pt ch	−5.0	−3.4	−4.9	−3.3	−24.9	6.6	0.3
Fe−C−N=120° + three 0.2 pt ch	−5.4	−4.5	−5.1	−4.0	−6.7	6.5	−1.1

more, the optimized Fe−S−C_β−C_α dihedral angles of ∼160° and ∼90° for the CN-SOR and CN-P450 models, respectively, are unaffected by constraining the thiolate ligand such that C_β bisects N1 and N4 (i.e., the N1−Fe−S−C_β dihedral angles = 45°). Thus, the enzymes appear to have evolved to support the active-site geometry with an optimal electronic energy.

The calculated electronic structures of the CN-SOR and CN-P450 models are very similar, despite the differences of the equatorial ligands, as shown by the contour plots of their frontier molecular orbitals (see Supporting Information). As expected based on optical and vibrational spectroscopic properties,[24,45] the unpaired electron of both models is in an iron d_π orbital that interacts with the p_π orbital of the cysteinyl sulfur and the π orbitals of the cyanide ligand. This bonding description is robust in that the relative energies and composition of the frontier molecular orbitals do not change significantly with any of the geometric perturbations explored in these calculations. Comparison of the singly occupied molecular orbital in each of the two models (Figure 8) shows that the overall calculated spin density distributions are similar for the two active-site models, with the majority of the spin density along the axis shared between the iron, sulfur, and cyano carbon atoms (Table 3). However, when inspected more closely, the on-axis spin distributions do differ by a small but meaningful amount, with CN-P450 showing greater spin density on iron and slightly less on sulfur than CN-SOR.

Fe−S−C_β−C_α Dihedral Angle. The axial spin densities in the two gas-phase models are similar (Table 3) but do show noticeable differences; the ρ_S = 0.309 for optimized CN-P450 is 30% smaller than ρ_S = 0.322 for CN-SOR. We did computations to test whether this difference reflects the different in-plane ligands or the ∼70° difference in the Fe−S−C_β−C_α dihedral angles of SOR and P450. We "swapped" the geometries of the alkyl-thiolate ligands of the two models by constraining the Fe−S−C_β−C_α dihedral angle and optimizing all other parameters. None of the other parameters changed appreciably (Table 2), nor did the spin densities change significantly. Conversion to the "hybrid" geometries only changed ρ_S of CN-SOR by ∼1% and ρ_S of CN-P450 by ∼6%. Thus, the differences between "on-axis" spin densities in the two models indeed reflect differences between the "in-plane" ligand sets of the two enzymes.

Fe−N Bonding and N_{eq} Hyperfine. The equatorial nitrogen spin densities are small and very similar in the two models. The calculated $a_{iso}(N_{eq})$ reproduce the asymmetries disclosed by the ENDOR spectra (Table 4). For CN-SOR, the a_{iso} of N1 determined by ^{14}N ENDOR, and assigned to His16 based on the quadrupole coupling, is larger than those of the other three equatorial nitrogens, and the DFT computations reproduce the result that His16 has the largest a_{iso} of the equatorial nitrogens. The two-fold symmetry of the heme, as indicated by the ^{14}N ENDOR of CN-P450cam, also is reproduced by the calculations. However, in both models, the calculated $a_{iso}(N_{eq})$ are systematically smaller than the experimental values, indicating an underestimate of the spin density on the in-plane ligands.

Fe−S Bonding and H_β Hyperfine. In both models, the calculated a_{iso} for the two cysteine H_β atoms are more than 3-fold larger than experiment. According to eq 2b, this indicates that the ρ_S calculated for the gas-phase models is correspondingly larger than the actual values in the enzymes. Despite this, the DFT computations support the essential accuracy of eq 2b and the semiempirical value(s) of *B*. By inserting the DFT values for ρ_S and a_{iso} into eq 2b, a DFT value for *B* can be calculated; for H1 this gives an average *B* = 115 MHz for CN-SOR and *B* = 93 MHz for CN-P450, in satisfactory agreement with the semiempirical values of *B* = 83/100 MHz and favoring the higher value. Thus, the calculations support the accuracy of the ρ_S values determined experimentally.

One can further use the DFT results to check the validity of the dependence of a_{iso} on the Fe−S−C_β−H dihedral angle that is explicitly included in eq 2b. This equation predicts that the ratio of isotropic couplings for H1 and H2 is determined solely by geometry:

$$\frac{a_{iso}(H1)}{a_{iso}(H2)} = \frac{[\sin^2 \theta'(1)]}{[\sin^2 \theta'(2)]} \quad (5)$$

Thus, a comparison of the ratio of the a_{iso}(H) from DFT with the ratio of the $\sin^2 \theta'$ from the X-ray structures is an appropriate test for the computations, regardless of the accuracy of the calculated values for ρ_S. This relation is well obeyed within reasonable error by both the experimental and calculated values of a_{iso}(H) for CN-SOR.[53] The calculations for CN-P450 are more variable, but the a_{iso}(H) are smaller, particularly for H2, and the deviation likely reflects the omission of a small constant term that in principle should be included in eq 2b.

Thus, overall, the analyses support the use of eq 2b and confirm that the difference between calculated and observed $^1H_\beta$ couplings reflects an overestimate of ρ_S in the "gas-phase" models. We address this issue further below, where we show that the measured values of a_{iso} are more closely reproduced by the calculations if one includes the influence of the H-bonding to the cysteine sulfurs that is present in both enzymes.

Fe−C−N Bonding and Cyanide ^{13}C Hyperfine. Geometry optimizations without constraints on the bend angle of the cyanide resulted in a nearly linear Fe−C−N linkage for both models (Table 2). The calculations give slightly more spin density on the iron atom of CN-P450 (Table 3), and this leads to a slightly higher calculated a_{iso}(C) of ∼22 MHz for CN-P450 vs ∼18 MHz for CN-SOR. The a_{iso}(C) for CN-SOR with linear Fe−C−N is 40% lower than that for the C1 ($\theta = 175°$) substate observed by ^{13}C ENDOR, indicating that spin delocalization onto the cyanide ligand is significantly underestimated in this gas-phase model. Taken together with the overestimates of a_{iso}(H) for the cysteinyl H_β atoms, both support the idea that spin delocalization from iron to sulfur is overestimated.

Fe−C−N Bending. The influence of bending the cyanide ligand was investigated with calculations on both enzyme models that constrained only the Fe−C−N angle (θ) over a range of 120°−80° ($\theta = \pi$). Figure 9 shows the DFT-calculated a_{iso} for the cyano carbon as the ligand bends (scaled as $^C a_{iso}(\theta)/^C a_{iso}(\pi)$) along with the value predicted by the rigid-orbital model of eq 3. The calculations qualitatively support this model in yielding a decrease in a_{iso}(C) as θ decreases, as seen in experiment. The correspondences between a_{iso} and θ for the rigid-orbital model and for the computations are similar for both models until $\theta \lesssim 140°$, where the DFT slope of a_{iso} vs θ becomes more steep. The steep slope in the DFT plot of a_{iso} *vs* θ beyond $\theta \lesssim 140°$ reveals the limitations to the rigid-orbital model. This model assumes that the spin densities on carbon and iron (and sulfur) are independent of the Fe−C−N angle, and that a_{iso}(C) decreases as θ decreases solely because of rehybridization of the cyano carbon; in fact, cyanide ligand bending also redistributes the on-axis spin density.

This on-axis spin density redistribution is seen in Figure 9, which depicts the θ dependence of the spin density on iron, sulfur, and the cyano carbon, presented as a fraction of the spin density for linear Fe−C−N ($\rho(\theta)/\rho(\pi)$). Plotted in this fashion, the variation of spin density with Fe−C−N angle is the same for the gas-phase and H bond models (vide infra). As the cyanide ligand bends and θ becomes less than ∼150°, the spin densities on both the carbon and sulfur atoms noticeably decrease, and the spin is transferred to the iron. This on-axis spin density

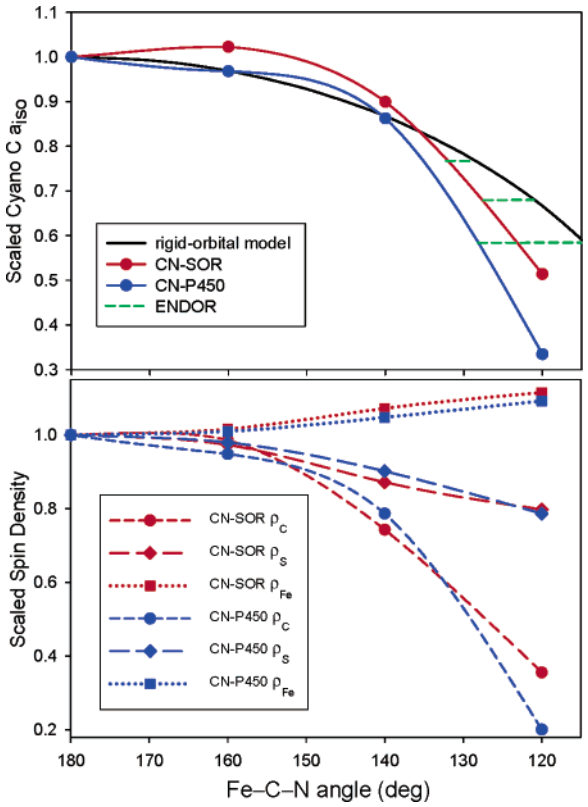

Figure 9. (Top) DFT-calculated a_{iso}(C) for the cyanide carbon scaled as $a_{iso}(\theta)/a_{iso}(\pi)$ versus Fe−C−N bend angle. (Bottom) Spin densities of on-axis atoms presented as a fraction of the spin density for linear Fe−C−N ($\rho(\theta)/\rho(\pi)$) as a function of Fe−C−N bend angle.

redistribution adds to the effect of rehybridization at the cyano carbon, leading to the steepened curve of a_{iso} vs θ. The on-axis spin redistribution caused by Fe−C−N bending does not significantly affect the average spin density on the equatorial nitrogens, although the average $a_{iso}(N_{eq})$ does increase by ∼1 MHz over the entire bend-angle range.

Hydrogen Bonding to the Sulfur. The above analysis for the gas-phase models indicates that the DFT computations greatly overestimate the spin density on sulfur and underestimate those on iron, the equatorial nitrogens, and cyano carbon. This results in discrepancies compared to experiment in which the calculated a_{iso} are too large for cysteinyl H_β atoms and too small for the cyano carbon and equatorial nitrogens. We speculated that these discrepancies occur because the gas-phase model does not incorporate H-bonding to cysteinyl sulfur. The crystal structures show that SOR has two and P450cam has three H bonds to the cysteine sulfur (Figure 10). As an initial effort to explore the influence of these interactions, we adopted a simple approach that has been used previously to model H-bonding interactions in P450 as static point charges.[54] The inclusion of partial positive point charges (each of equal magnitude, either 0.1, 0.2, or 0.3) in our calculations, located at the positions of the H-bonding atoms shown in the crystal structures, does not change the overall bonding description, but does stabilize the negative *charge* on the thiolate and decrease its delocalization to iron. This charge stabilization thereby decreases the spin density on sulfur and increases the spin density on iron, the cyano ligand, and equatorial nitrogens (Table 3). As a conse-

(53) The agreement is essentially perfect for the two CN-2Fe-SOR, with a ratio of ∼2.2, whereas the CN-1Fe-SOR agrees within 10%.

(54) Altun, A.; Guallar, V.; Friesner, R. A.; Shaik, S.; Thiel, W. *J. Am. Chem. Soc.* **2006**, *128*, 3924−3925.

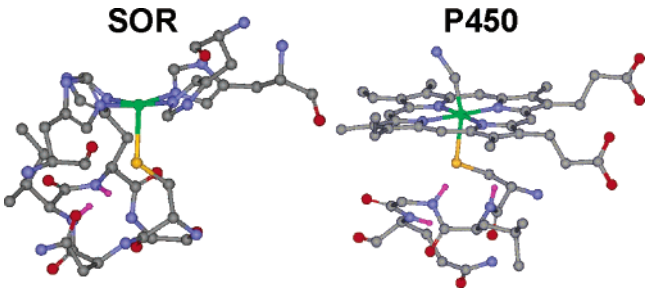

Figure 10. X-ray crystal structures of the SOR and P450cam active sites showing the H bonds to the cysteinyl sulfur that were modeled in the calculations as partial positive point charges at the coordinates corresponding to the H atom positions (magenta balls) shown. All other H atoms have been omitted for clarity.

quence of this, the corresponding a_{iso} of the equatorial nitrogens, cyano carbon, and cysteinyl β hydrogens (Table 4) are in better agreement with ENDOR results.

Discussion

SOR and P450 have active sites with the same first-shell coordination spheres and share a common ferric-(hydro)peroxy catalytic intermediate, but catalyze very different reactions. P450 catalyzes O_2 activation, and heterolytic O−O bonds cleave to yield a high-valent, $Fe^{IV}=O$ oxidizing species via a proposed low-spin Fe(III)−OOH intermediate,[9,10] whereas SOR catalyzes reduction of O_2^- to H_2O_2 without O−O bond cleavage.[1,6,11] Kinetic studies of SOR have identified a transient intermediate that is proposed to be a ferric-(hydro)peroxy species,[55−59] but there are conflicting reports concerning the spin state, protonation state, and (hydro)peroxy binding geometry. For example, DFT and ZINDO/S-CI results favor a low-spin, end-on ferric-(hydro)peroxy intermediate,[60] whereas a high-spin, side-on ferric-peroxy intermediate has been proposed on the basis of EPR, resonance Raman, Mössbauer, and DFT studies of a transient species generated on addition of H_2O_2 to reduced SOR.[61,62] Spectroscopic characterization of a range of ferric-alkylperoxo complexes[63−65] and the NO-adduct of reduced SOR[20] indicate that the Fe(III) spin state is likely to be a key determinant of the reactivity of ferric-(hydro)peroxy species, with high-spin stabilizing the peroxo species and low-spin favoring cleavage of the O−O bond. Additional factors that have been proposed to play a role in tuning the reactivity of the ferric-(hydro)peroxy intermediate include differences in the covalency of the $Fe-S_{Cys}$ bond, the dinegative charge of the heme ligand in P450 versus four neutral His ligands in SOR, the relative difficulty of forming a ligand cation radical from the four His ligands in SOR, and the much higher solvent exposure of the SOR site which favors protonation of both peroxo ligand oxygens and release of H_2O_2.[2,6,66]

In this work we have investigated the low-spin cyanide-bound ferric forms of SOR and P450cam using ENDOR spectroscopy and DFT calculations, in order to characterize the bonding of the common cysteinyl axial ligands and to explore the differences that result from the two different types of equatorial N_4 ligation: [histidyl-imidazole-N]$_4$ in SOR and [heme-pyrrole-N]$_4$ in P450cam. Cyanide was chosen as a potential mimic of the (hydro)peroxo axial ligand in order to assess the differences in bonding of low-spin forms of the common ferric-(hydro)-peroxy catalytic intermediate. The initial goal was broadened by the inclusion of DFT computational results. These disclosed that in the cyano-ferric state the influences of the different equatorial ligations in the two enzymes on the bonding to iron are apparent, but less than those of the H bonds to cysteinyl sulfur. Here we (a) summarize the differences between the experimental findings for the two enzymes, (b) discuss the differences between the computational findings for the gas-phase enzyme models, and (c) consider the consequences of introducing the influence of H bonds to cysteinyl sulfur.

The experimental finding is that there are small, but significant, differences in the bonding between Fe(III) and its ligands in the two enzymes. ^{14}N ENDOR of the coordinating nitrogens of CN-SOR and CN-P450cam give small average hyperfine coupling for both enzymes, with small differences in value which represent large percentage differences: $a_{iso}=4.5$ MHz for CN-1Fe-SOR, 5.6 MHz for CN-P450cam. Further, the deviations from the average are quite different for the two sites. Each of the four histidyl imidazole ligands of the CN-SOR site has a different dihedral angle relative to the Fe-N_4 plane, $\beta=$ 47° (His16), 36° (His 41), 85° (His47), 53° (His114), and this leads to a substantial distribution in ^{14}N hyperfine couplings at g_1, $a_{iso}=3.6-6.0$ MHz, variations of $\sim\pm30\%$ around the average. As is common for low-spin ferrihemes, the CN-P450cam heme also shows an apparent reduction in heme symmetry from four- to two-fold, with two types of ^{14}N, but the difference between the two values, $a_{iso}=5.2$ and 5.9 MHz, is much less than that between the four histidyl ligands of CN-SOR. In fact, this observation is inherent in the crystal-field analysis of the **g** tensors of the two enzymes. The largest distortion (elongation) from cubic symmetry in CN-P450cam is along the normal to the heme (*z*-axis), and the deviations from rotational symmetry around that axis, parametrized as V/Δ, are not large. In contrast, the canonical *z*-axis for CN-SOR lies in the N_4 plane.

While the differences between in-plane ^{14}N hyperfine couplings for the two enzymes are modest, these are accompanied by dramatic differences in the hyperfine couplings to the cysteinyl H_β protons of the two enzymes. The nonexchangeable H_β protons of the CN-SOR axial cysteinyl ligand have large isotropic hyperfine couplings, $a_{iso}(H1)\approx+14-17$ MHz and $a_{iso}(H2)\approx+7$ MHz. These hyperfine couplings are related to the spin density delocalized onto sulfur, ρ_s, through the semiempirical eq 2, which is based on a model in which spin density is transferred from sulfur to H_β by hyperconjugation.[46]

(55) Coulter, E. D.; Emerson, J. P.; Kurtz, D. M., Jr.; Cabelli, D. E. *J. Am. Chem. Soc.* **2000**, *122*, 11555−11556.
(56) Emerson, J. P.; Coulter, E. D.; Phillips, R. S.; Kurtz, D. M., Jr. *J. Biol. Chem.* **2003**, *278*, 39662−39668.
(57) Abreu, I. A.; Saraiva, L. M.; Soares, C. M.; Teixeira, M.; Cabelli, D. E. *J. Biol. Chem.* **2001**, *276*, 38995−39001.
(58) Lombard, M.; Houee-Levin, C.; Touati, D.; Fontecave, M.; Niviere, V. *Biochemistry* **2001**, *40*, 5032−5040.
(59) Niviere, V.; Lombard, M.; Fontecave, M.; Houee-Levin, C. *FEBS Lett.* **2001**, *497*, 171−173.
(60) Silaghi-Dumitrescu, R.; Silaghi-Dumitrescu, I.; Coulter, E. D.; Kurtz, J.; Donald M. *Inorg. Chem.* **2003**, *42*, 446−456.
(61) Mathe, C.; Mattioli, T. A.; Horner, O.; Lombard, M.; Latour, J.-M.; Fontecave, M.; Niviere, V. *J. Am. Chem. Soc.* **2002**, *124*, 4966−4967.
(62) Horner, O.; Mouesca, J.-M.; Oddou, J.-L.; Jeandey, C.; Niviere, V.; Mattioli, T. A.; Mathe, C.; Fontecave, M.; Maldivi, P.; Bonville, P.; Halfen, J. A.; Latour, J.-M. *Biochemistry* **2004**, *43*, 8815−8825.
(63) Lehnert, N.; Ho, R. Y. N.; Que, L., Jr.; Solomon, E. I. *J. Am. Chem. Soc.* **2001**, *123*, 12802−12816.
(64) Lehnert, N.; Ho, R. Y. N.; Que, L., Jr.; Solomon, E. I. *J. Am. Chem. Soc.* **2001**, *123*, 8271−8290.
(65) Bukowski, M. R.; Halfen, H. L.; van den Berg, T. A.; Halfen, J. A.; Que, L., Jr. *Angew. Chem., Int. Ed.* **2005**, *44*, 584−587.
(66) Kurtz, D. M. *J. Inorg. Biochem.* **2006**, *100*, 679−693.

The positive sign determined experimentally by applying the modified Davies/Hahn pulsed ENDOR sequence of Chart 1 implies that ρ_s is positive. Therefore, the H_β experimental couplings for the CN-SORs give $\rho_s = +0.17-0.20$. The positive sign of ρ_s confirms that the spin density on the axial sulfur is introduced by π delocalization rather than spin polarization of the Fe−S σ bond. This evidence of strong Fe−S covalency in the CN-SORs complements the earlier data from optical and vibrational spectroscopies of strong σ and π bonding between iron and sulfur, consistent with the metal−sulfur bonding in SORs being similar to that in blue-copper centers.[13,20] In addition, resonance Raman data for wild-type and cyanide-bound oxidized SOR indicate that negligible changes in the $Fe-S_{Cys}$ stretching frequency accompany the high-spin to low-spin transition that occurs when the glutamate trans ligand is replaced by cyanide. The results show that the solution active-site structures of SORs reflect the crystallographically determined structures and that cyanide ligation does not appreciably perturb these structures.

In contrast to the large $^1H_\beta$ isotropic hyperfine couplings observed for CN-SORs, the ^{1}H ENDOR pattern of CN-P450cam is narrow, $a_{iso} \lesssim 3$ MHz. The hyperfine couplings to protons of ferrihemes typically are small, with the largest coupling $\lesssim 1-2$ MHz, and hence the breadth of the pattern of CN-P450cam likely is determined by the $^1H_\beta$ couplings, which means that they are no less than 5-fold smaller than those of the CN-SORs. However, this difference is primarily due to the different geometry of the axial cysteine ligand which yields a much smaller value for the angle-dependent factor in eq 2, which reduces the $^1H_\beta$ coupling. Thus, according to this equation the spin density on the sulfur is $\rho_s \approx 0.14$ for CN-P450cam, ~2/3 that for the CN-SORs. At present there is neither optical nor vibrational evidence from cyano-ferric-P450cam for strong Fe−S covalency comparable to that seen in cyano-ferric-SORs. However, strong covalency is suggested by the $Fe-S_{Cys}$ bond lengths in high-resolution structures. Both the 5-coordinate high-spin ferric and 6-coordinate low-spin cyano-ferric forms of P450cam (2.36 and 2.37 Å, respectively),[10,15] have $Fe-S_{Cys}$ bonds which are ~0.1 Å shorter than reported for the 6-coordinate ferric-1Fe-SOR crystal structure (2.46 Å)[7] and about the same as the reported EXAFS-determined distance for 6-coordinate ferric-1Fe-SOR (2.36 Å).[13]

The *values* of the isotropic hyperfine couplings for ^{13}CN, $^{14}N_{eq}$, and ^{1}H (β-cysteinyl) obtained by DFT computations on the gas-phase models differ significantly for the two enzyme active-site models, in part because of the different dihedral angles (eq 2b) and in part because of differing spin densities. It was nonetheless possible to use these computations to test, and thus validate, the semiempirical eq 2b which relates $a_{iso}(H)$ to ρ_S for the cysteine ligand; both the dependence on $Fe-S-C_\beta-H$ dihedral angle and the value of the proportionality constant, *B*, are supported. However, we conclude that there are real discrepancies between the predictions of the gas-phase model and the properties of the enzyme active sites.

To determine the source of these discrepancies, as a first approximation we modeled the influence of H bonds to cysteinyl sulfur, two in SOR and three in P450, with partial charges at the H-atoms involved (Figure 10). The inclusion of these influences bring the DFT calculations into satisfactory semiquantitative agreement with experimental values, which clearly indicates that these secondary interactions are of major importance in determining the electronic structure of these enzyme active sites. The S → Fe charge donation is overestimated in the gas-phase models, and this donation is diminished when the *charge* on sulfur is stabilized. As the S → Fe donation of charge is accompanied by an Fe → S migration of spin, the gas-phase DFT calculations overestimate the $^1H_\beta$ hyperfine couplings. This active-site electronic-structure tuning phenomenon has been previously observed in the case of Compound I of P450, which has an $Fe^{IV}O$ coupled to a radical.[67] Gas-phase calculations predict the cysteinyl sulfur has given up nearly one full charge to become a sulfur radical, contrary to experiment, but with the inclusion of the secondary effects, those calculations achieved agreement with experiment. Likewise, a recent experimental study has indicated that N−H−S hydrogen-bonding significantly reduces Fe−S covalency in heme-thiolate complexes.[68] In principle, one might expect the spin density on the sulfur of P450, with three H bonds, to be reduced by H-bonding to a greater extent than in SOR, with two H bonds. To achieve the more exact correspondence between experiment and computation needed to address this refinement, more elaborate computations will be required.

Summary

This work has compared the properties of the iron ligands of CN-SOR and CN-P450cam through a combination of ^{1}H, ^{13}C, and ^{14}N ENDOR spectroscopy, discussed in a context provided by vibrational and structural studies. Further insight has been gleaned by DFT computations on gas-phase active-site models and models that incorporate the influence of H-bonding to the axial cysteinyl sulfur by protein. On a technical level, the combination of these approaches has: (i) determined the sign of the cysteinyl β-proton hyperfine coupling through a newly developed pulsed-ENDOR sequence (Davies/Hahn sequence); (ii) confirmed the applicability of the commonly used, semiempirical relation between spin density on sulfur and β-proton isotropic hyperfine couplings; (iii) improved our understanding of the consequences of bending the Fe−C−N linkage on the distribution of spin density over the "on-axis" atoms. On the chemical/biochemical level, this study has shown the following: (iv) the difference between the "in-plane" heme and "out-of-plane dihedral" His_4 ligation of P450cam and SOR, respectively, causes real differences in the distribution of spin density over the "on-axis" atoms; (v) introduction of H-bonding effects to the axial cysteinyl sulfur ligand reduces the spin density on the sulfur in both active sites to a degree that likely exceeds the difference caused by the different in-plane nitrogen ligands. The last two points provide a clear example that inclusion of electronic-structure tuning by H-bonding to the sulfur ligand is necessary for a complete determination of the active-site electronic structure of SOR and P450 enzymes.

Acknowledgment. We thank Professor John Dawson for the samples of CN-P450cam and Irene Y. Kung for preparation of the CN-SOR samples. This work was supported by grants from the National Institute of Health (GM067349 to R.L.M.; GM60329 to M.K.J. and M.W.W.A.; GM40388 to D.M.K.; and HL13531 to B.M.H.)

(67) Schoneboom, J. C.; Neese, F.; Thiel, W. *J. Am. Chem. Soc.* **2005**, *127*, 5840−5853.
(68) Dey, A.; Okamura, T.; Ueyama, N.; Hedman, B.; Hodgson, K. O.; Solomon, E. I. *J. Am. Chem. Soc.* **2005**, *127*, 12046−12053.

Supporting Information Available: Two-dimensional field dependent ^{13}C CW ENDOR of ^{13}CN-P450cam, molecular orbital contour plots of selected CN-SOR and CN-P450 frontier orbitals, and complete tables of DFT calculation results. This material is available free of charge via the Internet at http://pubs.acs.org.

JA064656P